ELSEVIER

Journal of Nuclear Materials 219 (1995) 152–160

journal of nuclear materials

Effects of concurrent irradiation with ions and electrons on the formation process of defect clusters in covalent and ionic crystals

C. Kinoshita [a], H. Abe [b], S. Maeda [a], K. Fukumoto [c]

[a] *Department of Nuclear Engineering, Kyushu University 36, Fukuoka 812, Japan*
[b] *Department of Materials Development, Takasaki Establishment, Japan Atomic Energy Research Institute, Takasaki, Gunma 370-12, Japan*
[c] *Institute for Material Research, Tohoku University, Sendai 980, Japan*

Abstract

In order to understand concurrent effects of damage cascades, isolated point defects and ionization on the formation process of defect clusters in covelent and ionic crystals, in-situ observations of Ge, Si and $MgAl_2O_4$ crystals have been performed under dual-beam irradiation with ions and electrons in the HVEM accelerator facility at Kyushu University. Damage cascades in the covalent crystals show up their contrast through overlap or help from other damage cascades. Simultaneous electron irradiation eliminates damage cascades in the covalent crystals through the irradiation-induced and -enhanced migration of point defects. In the ionic crystal, on the other hand, no damage cascades show up their contrast, but interstitial loops are formed through the nucleation and growth process. Effects of concurrent irradiation with ions and electrons on this process are based on defect reactions among damage cascades and isolated point defects. Homogeneous ionizing radiation plays no significant role on the nucleation and growth process of defect clusters.

1. Introduction

Fast neutrons transfer their kinetic energy to primary knock-on atoms (PKAs), producing PKAs with a variety of energies. The PKAs introduce not only damage cascades but also other elementary defects such as isolated point defects, irradiation-induced migration of point defects and ionization [1,2]. Therefore, it is important to understand the concurrent effect of those elementary processes on the accumulation process of damage cascades. Dual-beam irradiation with ions and electrons provides independent factors controlling radiation damage processes; heavy ions with energies of several tens keV generate primarily damage cascades in contrast to fast electrons which induce isolated point defects, ionization and athermal migration of point defects. Thus, dual-beam irradiation gives important information on the concurrent effect of those elementary processes on accumulation, structure and stability of damage cascades [3].

The first objective of the present paper is to get insights into the concurrent effect of damage cascades, isolated point defects and/or ionization on the accumulation process of defect clusters in Ge and Si. The second one lies on understanding the concurrent effect of atomic displacements and ionization on the nucleation and growth process of defect clusters in $MgAl_2O_4$.

2. Experimental procedures

Single crystals of Ge, Si and $MgAl_2O_4$ were supplied by Sumitomo Met. Min. Co., Kyushu Elec. Co. and Union Carbide Co., respectively. They were cut into 3 mm diameter discs with an ultrasonic cutter and mechanically polished to get the thickness of ~ 200 μm. Polished discs were dimpled into ~ 30 μm in thickness at the center of the discs. Ge and Si discs were further thinned to TEM foils with chemical polishing solutions [4] at room temperature, then rinsed in water, methanol and ethanol in that order. $MgAl_2O_4$ discs were subjected to ion thinning with 6 keV Ar^+ ions whose incident angle was 20° from the surface of discs by using a cold stage cooled by liquid nitrogen,

0022-3115/95/$09.50 © 1995 Elsevier Science B.V. All rights reserved
SSDI 0022-3115(94)00389-0

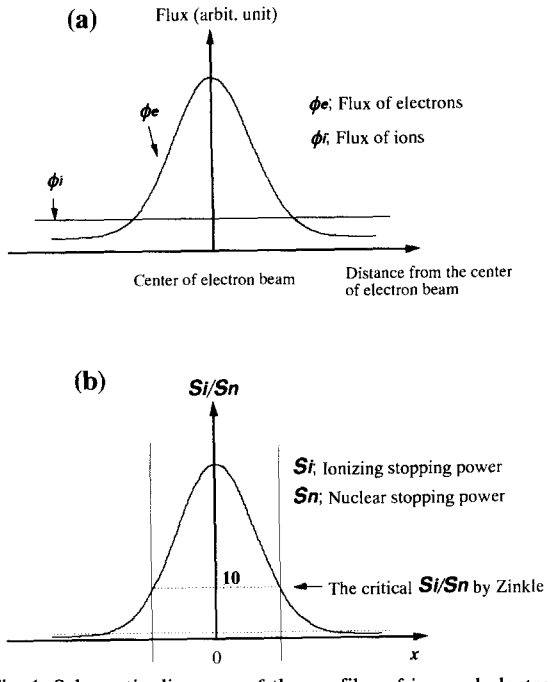

Fig. 1. Schematic diagrams of the profiles of ion and electron fluxes (a) and of the positional distribution of the ratio of ionizing to displacive stopping powers, S_i/S_n (b). The critical value of S_i/S_n is explained in Section 4.

until perforation occurred ($\sim$ 20 h). The final polishing for $MgAl_2O_4$ was performed for 1 h with 4 keV Ar^+ ions whose incident angle was 14°. The ion-thinned discs were annealed at 1670 K for 2 h in air with an electric furnace to remove defects and Ar atoms introduced by ion-thinning. During annealing, the discs were put in a small Al_2O_3 crucible to minimize contamination.

The thin foil specimens of Ge and Si were subjected to irradiation with homogeneous ion and electron beams in the HVEM accelerator facility at Kyushu University [2,5]. The accumulation process of damage cascades in Ge and Si was examined under irradiation with 30 keV Xe^+, 30 keV Ar^+ or 60 keV Ar^{2+} ions at room temperature. Relatively low ion fluences, less than 10^{17} ions/m^2, were used with various ratios of the 1 MeV electron flux (10^{22}–10^{23} e/m^2 s) to the ion flux ($\sim 10^{15}$ ions/m^2 s). Concurrent irradiation of the annealed $MgAl_2O_4$ specimens was performed with a focused 1 MeV electron beam and a homogenous ion beam such as 30 keV He^+, Ar^+ or Xe^+ ions. The profile of flux of the focused electron beam showed a Gaussian distribution, but the profile of ion flux was almost uniform, as schematically shown in Fig. 1a. Depending on the flux profile of electrons, therefore, there is a positional distribution of the radio of ionizing to displacive irradiation or the ratio of ionizing to nuclear stopping powers (S_i/S_n) shown in Fig. 1b. The nuclear and ionizing stopping powers of electrons were calculated from McKinley–Feshbach [6] and Bethe [7] formulas, respectively. The nuclear and ionizing stopping powers of ions were based on the TRIM code [8].

The ion current was measured with a Faraday cup which has an aperture with diameter of 200 mm, located at the specimen position of a specimen holder.

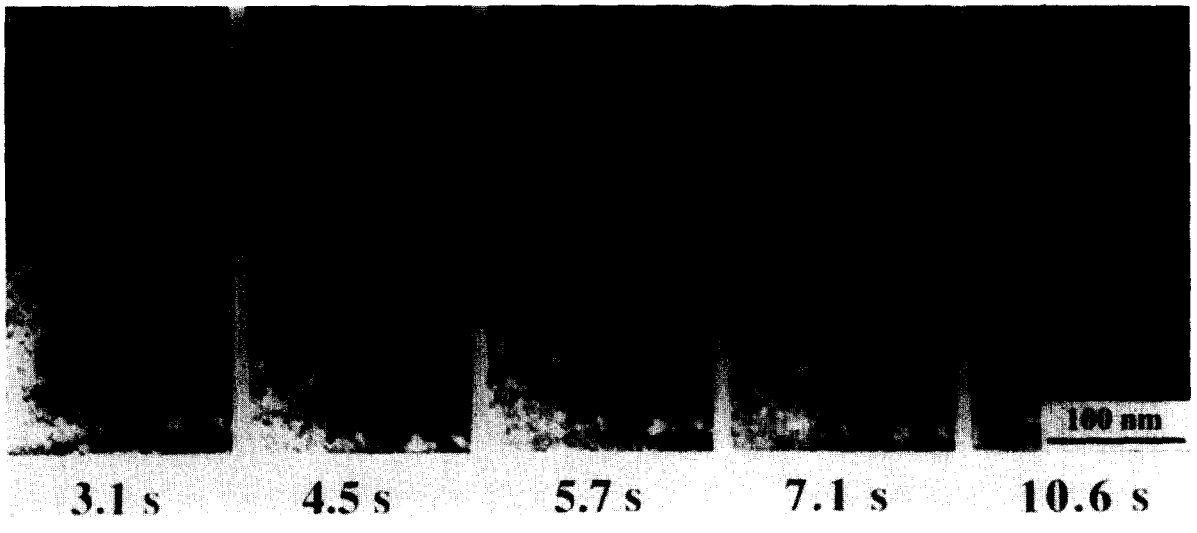

Fig. 2. A sequence of weak-beam dark-field images on a TV monitor showing the evolution of cascade contrast in Ge irradiated with a 30 keV Xe^+ flux of 5.0×10^{15} ions/m^2 s and a 1 MeV electron flux of 1.8×10^{23} e/m^2 s. Some of the cascade contrast features indicated by arrows disappeared during irradiation.

3. Accumulation process of damage cascades in Ge and Si under concurrent irradiation with ions and electrons

Tiny defect clusters were observed in Ge and Si irradiated with 30 keV Xe^+ ions even at very low ion fluence of less than 10^{15} ions/m^2. Most of these contrast features may be attributable to amorphous zones [9–12], which essentially means that they correspond to damage cascades; such contrast will be referred as 'cascade contrast' in this paper. Fig. 2 shows sequential micrographs showing accumulation of cascade contrast in Ge irradiated with 30 keV Xe^+ ions. Damage cascades show up their contrast and increase in their number with irradiation time. The electron irradiation induces no significant change in cascade contrast features at the early stage of irradiation. However, continuous ion and electron irradiation annihilates some of cascade contrast as indicated with arrows in the figure. The annihilation can be observed through shrinkage of cascade contrast features.

The areal density of the cascade contrast was measured to clarify the effect of concurrent irradiation with ions and electrons on the accumulation process of damage cascades. Fig. 3 shows typical accumulation curves of the areal density of damage cascades in Ge irradiated with 30 keV Xe^+ ions. The values of the longitudinal axis in Fig. 3 are the fractional area of cascade contrast regions to fit the data with kinetic equations which will be described later. In those experiments the statistical error of the areal density ranges from 30 to 10% in accordance with the fraction from 10^{-3} to 10^{-1}, which almost corresponds to the areal density from 10^{14} to 10^{16}/m^2, while the error of irradiation time is less than 0.5 s. The cascade contrast increases in number within a few seconds, following $(\phi_i t)^x$ at the early stage of irradiation, where ϕ_i and t are ion flux and irradiation time, respectively. The values of x are estimated to be 1.0–1.7 for Ge irradiated with 30 keV Xe^+ ions, indicating that some of the damage cascades induce cascade contrast directly and others induce cascade contrast via the overlap of damage cascades or help from other damage cascades. The mechanism whereby neighboring damage cascades assist the formation of a visible amorphous zone is uncertain; it may be a plasticity spike (shock wave [13]) or a substantial flux from other damage cascades.

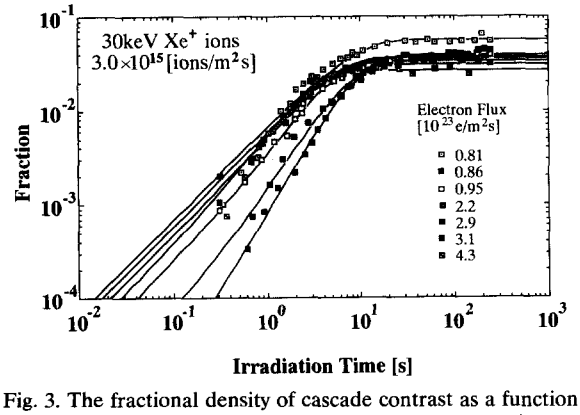

Fig. 3. The fractional density of cascade contrast as a function of irradiation time in Ge irradiated with 30 keV Xe^+ ions and 1 MeV electrons. The solid lines are the parametric fitting curves based on the kinetic equations (Eq. (1) or (2)).

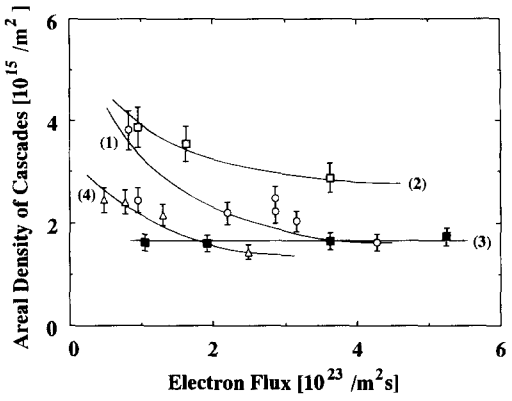

Fig. 4. The saturated areal density of damage cascades in Ge and Si as a function of 1 MeV electron flux for various irradiation conditions. (1) Ge irradiated with a nominal 30 keV Xe^+ flux of 3.0×10^{15} ions/m^2 s. (2) Ge irradiated with an actual 30 keV Ar^+ flux higher than 2.3×10^{15} ions/m^2 s. (3) Ge irradiated with an actual 30 keV Ar^+ flux lower than 2.3×10^{15} ions/m^2 s. (4) Si irradiated with a nominal 60 keV Ar^{2+} flux of 2.2×10^{14} ions/m^2 s.

In contrast to the early stage of the accumulation process, clearly shown in Fig. 3 is a decrease in the saturation density with increasing electron flux. This is a kind of concurrent effect of electron irradiation on the accumulation process of damage cascades. The annihilation of cascade contrast is presumably caused by both irradiation-enhanced and -induced diffusion of point defects. Here, the term 'irradiation-induced diffusion' means the diffusion induced by the direct or indirect collision of incident particles, and it is distinguished from 'irradiation-enhanced diffusion' which consists of the enhancement of thermally activated diffusion through the increase of diffusion carriers. The areal density at the saturation levels is plotted as a function of electron flux in Fig. 4 for Ge irradiated with 30 keV Xe^+ ions together with that for Ge and Si irradiated with 30 keV Ar^+ or 60 keV Ar^{2+} ions. The saturated density decreases with increasing electron flux. The electron flux dependence of the saturated density is related to the stability of damage cascades under simultaneous electron irradiation. The induced and enhanced diffusion of point defects during electron irradiation results in the shrinkage of damage

cascades. As will be revealed in the following, the saturated density depends not only on electron flux but also on actual ion flux. Some of the data in Fig. 4 show no dependence of electron flux on the saturated density of damage cascades, which might be caused by very low actual ion fluxes in Ge though the nominal flux is 2.3×10^{15} ions/m^2 s. Here, the nominal ion flux is defined as the averaged ion flux passed through an aperture (200 μm diameter) of the Faraday cup. On the contrary, the actual ion flux is defined as the ion flux evaluated from analyses of the experimental data based on the kinetic equations which will be described later. The lower ion flux gives the lower rate of cascade accumulation. Many of the damage cascades are annihilated by electron irradiation and/or thermal annealing without exhibiting their contrast.

Based on the previous discussion, we construct kinetic equations which describe the effect of simultaneous electron irradiation on the accumulation process of damage cascades. A fraction c of damage cascades creates a sufficiently high density of defects around the trajectory of ions and the regions are altered directly into the cascade contrast regions. The remaining fraction of cascades $(1-c)$ creates 'pre-damaged' regions, which transform into the cascade contrast regions via the overlap of damage cascades or the help from other damage cascades. Electrons induce the retardation of accumulation of damage cascades. The annihilation of amorphous and 'pre-damaged' regions contributes to the increase of undamaged regions. The variation of the fraction of cascade contrast regions C_A, that of 'pre-damaged' regions C_D and that of undamaged regions C_U under dual-beam irradiation with ions and electrons is given by

$$\frac{dC_A}{dt} = P_i C_D + cP_i C_U - P_e C_A,$$

$$\frac{dC_D}{dt} = -P_i C_D + (1-c)P_i C_U - P_e C_D,$$

and

$$\frac{dC_U}{dt} = -P_i C_U + P_e(C_A + C_D), \tag{1}$$

where the parameters P_i and P_e represent the cascade generation rate and the cascade annihilation rate, respectively, and c represents the fraction of damage cascades that result directly in the formation of cascade contrast regions. The parameter P_i is described as the ion flux ϕ_i when one ion induces one damage cascade, and P_e is proportioned to the electron flux ϕ_e required to annihilate a damage cascade. The terms $P_e C_A$ and $P_e C_D$ correspond to the annihilation of cascade contrast regions and 'pre-damaged' regions, respectively. The solution of the simultaneous differential equations for C_A is described with the initial and the boundary conditions ($C_A = C_D = 0$ at $t = 0$ and $C_A + C_D + C_U = 1$) as

$$C_A = \frac{P_i(P_i + cP_e)}{(P_i + P_e)^2}\left[1 - \left\{1 + \frac{P_i(P_i + P_e)(1-c)}{P_i + cP_e}t\right\} \times \exp\{-(P_i + P_e)t\}\right]. \tag{2}$$

From Eq. (2), the saturation level C_A^0 is expressed as functions of P_i, P_e and c by

$$C_A^0 = \frac{P_i(P_i + cP_e)}{(P_i + P_e)^2}. \tag{3}$$

The time variation of C_A was calculated from Eq. (2) for various combinations of the parameters P_i, P_e and c, and it is shown in Figs. 5a, 5b and 5c, respectively. Each result shows the accumulation of cascade contrast regions eventually leading to saturation. The parameter P_i affects the accumulation rate and the saturation level. With increasing value of P_i, the accumulation rate and the saturation level become higher. As for the parameter P_e, its effect is mainly on the saturation level; lower saturation levels occur for higher values of P_e. A slight difference in the initial slope of the accumulation process can be seen for different values of P_e in the figure. The initial slope of the accumulation process is mainly affected by the parameter, c, as seen in Fig. 5c. The lower value of c provides the higher accumulation rate of cascade contrast regions. The parameter c also affects the saturation level slightly.

It is possible to extend Eq. (2) to multiple overlaps of damage cascades [14] assuming that electrons annihilate the 'pre-damaged' regions with the same efficiency regardless of the number of overlaps (n) and that the parameter c is not incorporated. The time variation of C_A is also shown in Fig. 5c as a function of n. For $n > 2$, the initial slope of the accumulation process is larger than 2 in the figure, i.e. $x = 2.7$, 4.3 and 5.1 for $n = 2$, 4 and 6 in the relation $C_A \propto (\phi_i t)^x$, respectively. Since the value of x for experimental data is between 1 and 2, the multiple overlap model is not applied to the experimental data.

Eq. (2) describes the accumulation process of cascade contrast regions and the annihilation process. The solid lines in Fig. 3 are calculated from Eq. (2) so as to provide the best fit to the experimental results with the use of the least square method. The value of P_e thus obtained is plotted as functions of P_i and electron flux in Fig. 6. The parameters, P_i and P_e, are the accumulation rate and the annihilation rate of damage cascades, respectively. The parameter P_i is the product of the cross section required for damage cascades and the actual ion flux, and P_e is primarily that of the cross

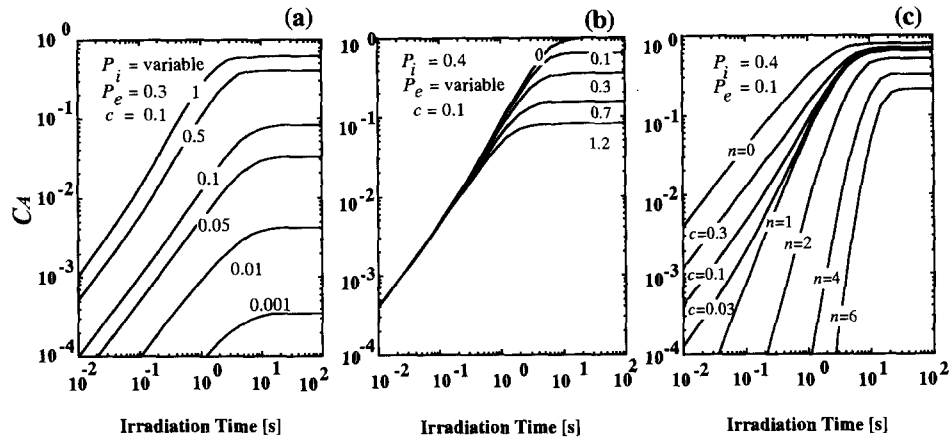

Fig. 5. The fractional variation of cascade contrast regions, C_A, as a function of irradiation time calculated from the kinetic equations or Eq. (1), adopting possible values for parameters P_i (a), P_e (b) and c and n (c).

section required for the cascade annihilation and the electron flux. The value of P_e increases with increasing electron flux, showing its higher electron flux dependence for the higher value of P_i under irradiation with 30 keV Ar^+ or Xe^+ ions. Those results indicate that 1 MeV electrons retard the accumulation of damage cascades through the irradiation-induced production of isolated point defects and their subsequent migration and that the retardation effect of electrons is relatively higher for the higher production rate of damage cascades. The finite value of P_e under ion irradiation without electrons might be attributed to the annealing effect of damage cascades themselves through migration of point defects within cascades.

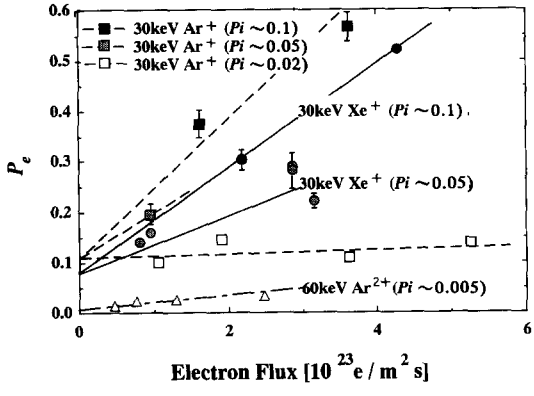

Fig. 6. The relation between cascade annihilation rate (P_e) and electron flux for Ge (solid lines and dashed lines) and Si (dot-dashed line) irradiated under various values of P_i. The values were obtained from Eq. (2) so as to provide the best fit to the experimental data shown in Fig. 3 as examples.

4. Microstructural evolution in $MgAl_2O_4$ under concurrent irradiation with ions and electrons

The HVEM accelerator facility has been applied to the dynamical in-situ observation of microstructural evolution in various kinds of crystals under irradiation at room temperature with 30 keV Xe^+ ions and 250 keV electrons. No contrast corresponding to individual damage cascades was observed in $MgAl_2O_4$, but interstitial loops appeared through the nucleation and growth process of defect clusters after irradiation up to high fluence levels [15]. In-situ observations were performed under simultaneous irradiation with a homogeneous 30 keV ion beam and a focused 1 MeV electron beam to investigate the concurrent effect of displacive and ionizing irradiation. Fig. 7 is a collection of weak-beam dark-field electron micrographs showing the sequential evolution of microstructures inside and outside the electron beam during irradiation with 30 keV He^+ ions and 1 MeV electrons at 870 K. The values of S_i/S_n were estimated to be 500 and 6 inside and outside the electron beam, respectively. Defect clusters appear both inside and outside the electron beam after irradiation for about 100 s and increase their density with increasing irradiation time. Defect clusters which are observed as dot contrast grow into well defined loops. No significant differences between the formation process of defect clusters inside and outside the electron beam are seen except for their density. The areal density of defect clusters is shown in Fig. 8 as a function of irradiation time, comparing the inside and outside of the electron beam. The areal density increases at early stage of irradiation, and then tends to saturate. The nucleation rate and the saturation density of defect clusters inside the electron beam are larger than those outside the electron beam. In the

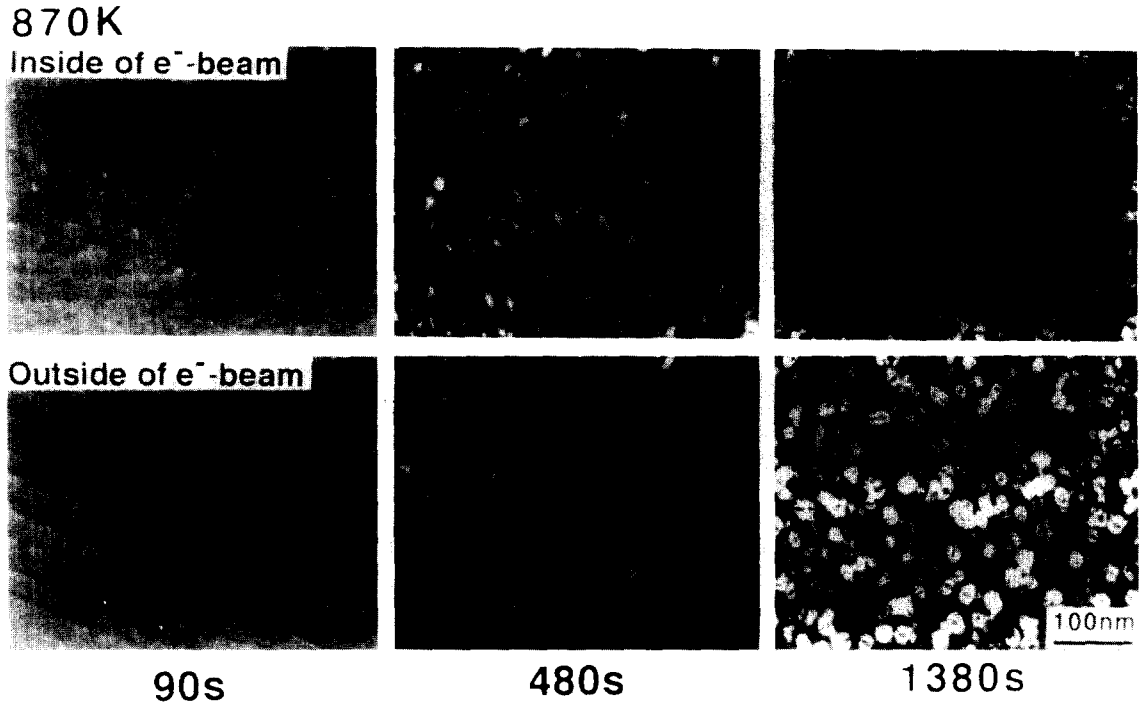

Fig. 7. Weak-beam dark-field images showing the sequential microstructural evolution inside and outside a focused electron beam during irradiation with 30 keV He^+ ions and 1 MeV electrons at 870 K. The fluxes of ions and electrons at the center of the electron beam were 4.0×10^{16} ions/m^2 s and 3.9×10^{23} e/m^2 s, respectively.

case of irradiation at 670 K, small defect clusters were formed and the difference between microstructures inside and outside the electron beam was not significant.

Analogous microstructural evolution was observed under irradiation with a homogeneous 30 keV Ar^+ and a focused 1 MeV electron beam at 870 K and is compared inside ($S_i/S_n = 60$) and outside ($S_i/S_n = 0.3$) the electron beam in Fig. 9. Defect clusters are formed irrespective of the inside and the outside of the electron beam and increase their diameter and density under irradiation. Fig. 10 shows the irradiation time dependence of the areal density of defect clusters inside and outside the electron beam. The nucleation process is analogous to that under irradiation with He^+ ions and electrons, though the difference in the areal density between the inside and the outside is not significant at the early stage of irradiation. Fig. 11 shows weak-beam dark-field images of microstructures inside ($S_i/S_n = 14$) and outside ($S_i/S_n = 0.2$) an electron beam in $MgAl_2O_4$ irradiated at 870 K to a 30 keV Xe^+ ion fluence of 1×10^{19} ions/m^2 and a 1 MeV electron fluence of 1.8×10^{26} e/m^2 inside the electron beam. The formation process of defect clusters under irradiation with Xe^+ ions is similar to that with Ar^+ ions, though defect clusters appear relatively soon after starting irradiation. The density of defects scarcely depends on the intensity or the position of the electron beam.

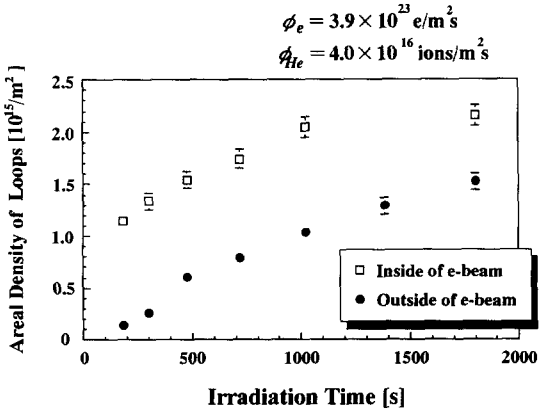

Fig. 8. The irradiation time dependence of the areal density of dislocation loops in $MgAl_2O_4$ under irradiation with a homogeneous 30 keV He^+ ion beam and a focused 1 MeV electron beam at 870 K, comparing the inside and the outside of the electron beam.

Recently, Zinkle [16] pointed out the importance of the ionizing to displacive ratio and observed no defect clusters around the higher ionizing region in $MgAl_2O_4$ irradiated with high energy light ions (e.g. 1 MeV He^+

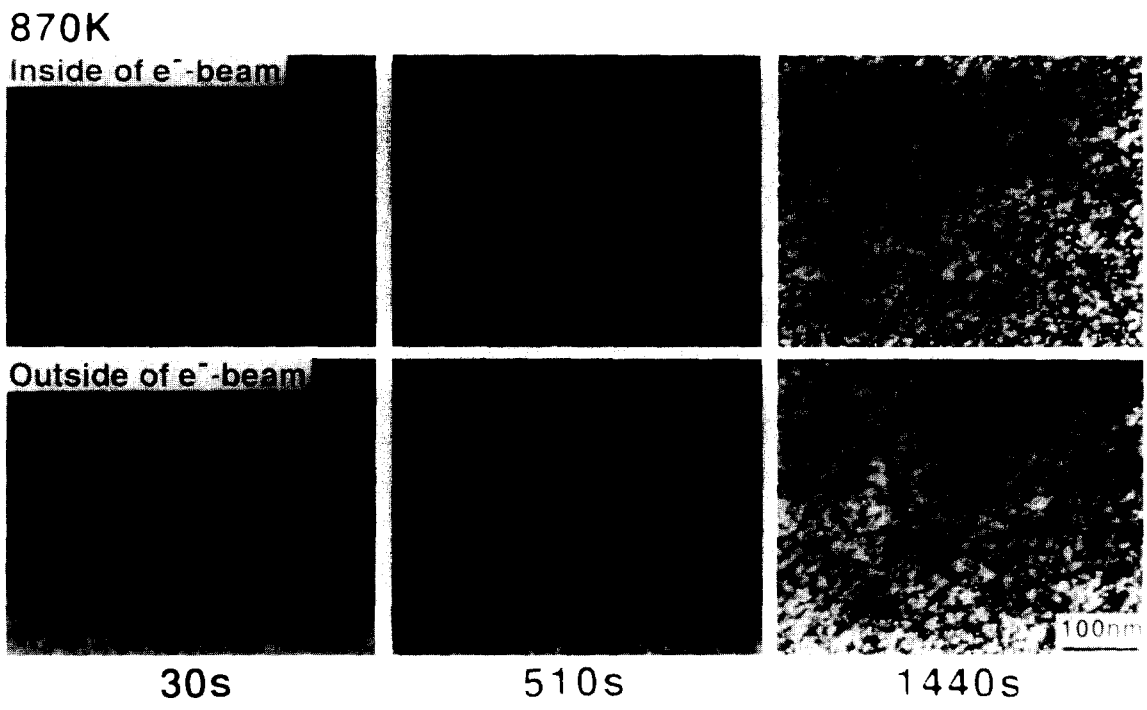

Fig. 9. Weak-beam dark-field images showing the sequential evolution inside and outside of a focused electron beam during irradiation at 870 K with a 30 keV Ar^+ ion flux of 2.0×10^{16} ions/m^2 s and a 1 MeV electron flux of 4.3×10^{23} e/m^2 s.

ions). According to Zinkle's criterion, the formation of defect clusters is expected to be suppressed inside the electron beam where the ratio of ionizing to nuclear stopping powers (S_i/S_n) is higher than 10 as schematically shown in Fig. 1, because of ionization-enhanced diffusion. In this study, no suppression effects of ionization on the formation of defect clusters was observed. Zinkle, however, used high energy heavy ions such as 1 MeV He^+ and Ar^+ ions, which induce highly localized ionization. In the concurrent irradiation with 30 keV ions and 1 MeV electrons, on the other hand, ionization is mainly due to electrons and is distributed homogeneously in contrast to localized damage cascades induced by the ions. Hence, the value of S_i/S_n under the concurrent irradiation is much smaller than that along the path of 1 MeV ions, even if average values of S_i/S_n are the same in both experiments. Therefore, the ionization effect on the formation of defect clusters during concurrent irradiation cannot be evaluated in terms only of the parameter S_i/S_n. However, the possible impact of the implanted ions on the preferential nucleation of defect clusters requires further study, referring to the results which show the importance of implanted ion effects on the microstructural evolution [17].

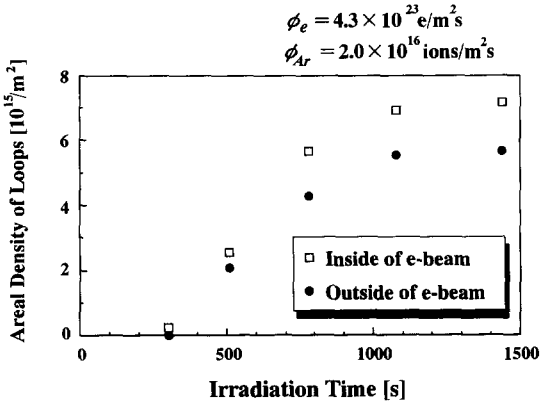

Fig. 10. The irradiation time dependence of the areal density of dislocation loops in $MgAl_2O_4$ under irradiation with a homogeneous 30 keV Ar^+ ions and a focused 1 MeV electron beam at 870 K, comparing the inside and the outside of the electron beam.

One MeV electrons themselves induce no defect clusters in $MgAl_2O_4$ [15] but enhance the nucleation of defect clusters under concurrent irradiation with ions, with the stronger effect observed for the lighter ions. Ions produce a high concentration of point defects within cascade regions which is favorable for the nucleation of defect clusters. The lighter ions, however, produce lower concentration of point defects within the larger cascade regions, forming a larger number of small subcascades. Furthermore, the average displacement rates under irradiation with 30 keV He^+, Ar^+

and Xe^+ ion fluxes of 2×10^{16} ions/m^2 s are estimated to be 3×10^{-5}, 7×10^{-4} and 2×10^{-3} dpa/s, respectively, in contrast to 5×10^{-4} dpa/s through 1 MeV electrons of 3×10^{23} e/m^2 s which is a typical flux of the concurrent irradiation experiments. Based on the experimental results and discussion, therefore, the nucleation process of defect clusters in $MgAl_2O_4$ shows a synergistic effect under concurrent irradiation with He^+ or Ar^+ ions and electrons, though it is controlled only by Xe^+ ions under irradiation with Xe^+ ions and electrons.

5. Conclusions

The HVEM accelerator facility has been extensively used for obtaining insights into the structure and the stability of damage cascades in Ge, Si and $MgAl_2O_4$ and into the concurrent effect of damage cascades, isolated point defects and/or ionization on the accumulation process of damage cascades or defect clusters. Concluding remarks are summarized as (1), (2) and (3) for Ge and Si and as (4) and (5) for $MgAl_2O_4$.

(1) Damage cascades produce observable TEM contrast in Ge and Si at the early stage ($< 10^{15}$ ions/m^2) of irradiation with 30 keV Xe^+, 30 keV Ar^+ and 60 keV Ar^{2+} ions, and they accumulate with increasing ion fluence following $(\phi_i t)^x$, eventually leading to saturation. The value of the power x depends on the combination of projectiles and target materials. The observed supralinear values for x indicate that some of the damage cascades directly produce cascade contrast, and others produce cascade contrast through the overlap of damage cascades and/or through the help from other damage cascades, i.e., shock wave (plasticity spike).

(2) The effect of concurrent irradiation with electrons and ions in Ge and Si is realized as the retardation of the accumulation of cascade contrast. Some of the cascade contrast disappears under continuous irradiation through their shrinkage without any structural change like loop formation. The areal density eventually saturates and the saturated density decreases with increasing electron flux.

(3) Kinetic equations have been developed to model the formation of cascade contrast regions via a cascade-overlap process, modified by an electron-damage component that serves to eliminate 'pre-damaged' and cascade contrast regions. The model well describes the observed phenomena.

(4) The low density and homogeneous ionizing radiation plays no significant role on the formation process of defect clusters in $MgAl_2O_4$.

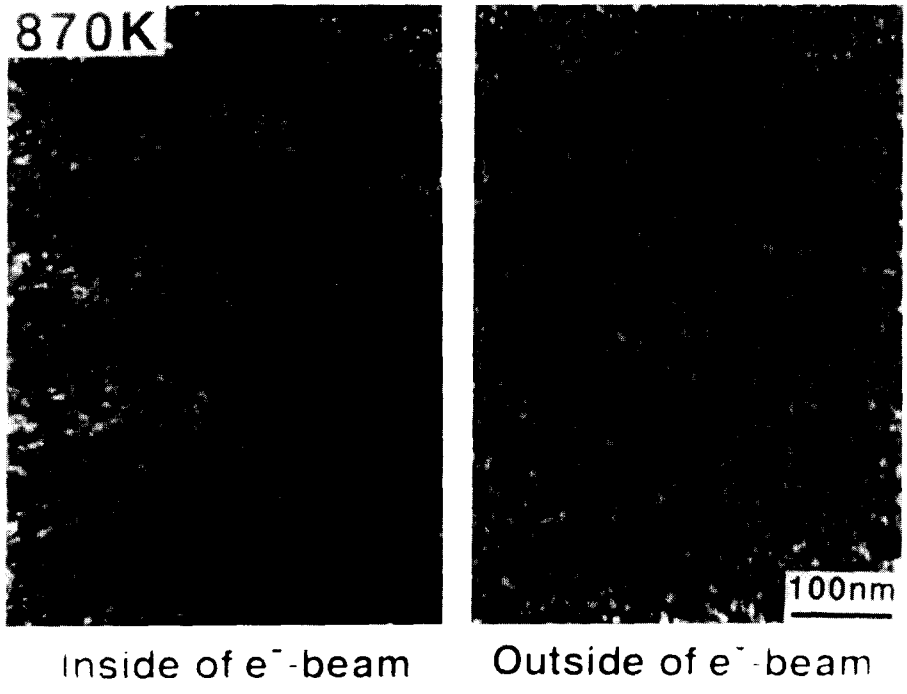

Fig. 11. A pair of weak-beam dark-field micrographs comparing microstructures inside and outside a focused electron beam in $MgAl_2O_4$ irradiated at 870 K with a 30 keV Xe^+ ion fluence of 1×10^{19} ions/m^2 and a 1 MeV electron fluence of 1.8×10^{26} e/m^2 at the center of the electron beam.

(5) The volume-averaged ionizing to displacive ratio S_i/S_n is not always a good parameter for describing the ionization effect on the formation of defect clusters in dual-beam irradiated ionic crystals.

References

[1] H. Abe, C. Kinoshita and K. Nakai, J. Nucl. Mater. 179–181 (1991) 917.
[2] K. Fukumoto, C. Kinoshita, H. Abe, K. Shinohara and M. Kutsuwada, J. Nucl. Mater. 179–181 (1991) 935.
[3] C. Kinoshita, Y. Isobe, H. Abe, Y. Denda and T. Sonoda, J. Nucl. Mater. 206 (1993) 341.
[4] C.A. Ferreira Lima and A. Howie, Philos. Mag. 34 (1976) 1057.
[5] C. Kinoshita, H. Abe, K. Fukumoto, K. Nakai and K. Shinohara, Ultramicroscopy 39 (1991) 205.
[6] W.A. McKinley and H. Feshbach, Phys. Rev. 74 (1948) 1759.
[7] H. Bethe and J. Ashkin, in Experimental Physics, vol. 1, ed. E. Segre (Wiley, New York, 1953) p. 166.
[8] J.F. Ziegler, J.P. Biersack and U. Littmark, in Stopping and Range of Ions in Solids (Pergamon, Oxford, 1985).
[9] L.M. Howe and M.H. Rainville, Nucl. Instr. and Meth. 182–183 (1981) 143.
[10] L.M. Howe and M.H. Rainville, Nucl. Instr. and Meth. B 19–20 (1987) 61.
[11] M.O. Ruault, J. Chaumont and H. Bernas, Nucl. Instr. and Meth. 170 (1980) 419.
[12] M.O. Ruault, J. Chaumont, J.M. Penisson and A. Bourret, Philos. Mag. A 50 (1984) 667.
[13] M. Guinan, J. Nucl. Mater. 53 (1974) 171.
[14] H. Abe, Eng. D. Thesis, Kyushu University (1993).
[15] Y. Satoh, C. Kinoshita and K. Nakai, J. Nucl. Mater. 179–181 (1991) 399.
[16] S.J. Zinkle, Fusion Reactor Materials Semiann. Prog. Rep. DOE/ER-0313/10 (1991) p. 302.
[17] S.J. Zinkle, Nucl. Instr. and Meth. B 91 (1994) 234.